DOI: 10.1002/cmdc.200600185

Understanding Binding Selectivity toward Trypsin and Factor Xa: the Role of Aromatic Interactions

Armida Di Fenza,[a] Andreas Heine,[a] Ulrich Koert,[b] and Gerhard Klebe*[a]

A congeneric series of four bis-benzamidine inhibitors sharing a dianhydrosugar isosorbide scaffold in common has been studied by crystal structure analysis and enzyme kinetics with respect to their binding to trypsin and factor Xa. Within the series, aromatic interactions are an important determinant for selectivity discrimination among both serine proteases. To study the selectivity-determining features in detail, we used trypsin mutants in which the original binding site is gradually substituted to finally resemble the factor Xa binding pocket. The influence of these mutations has been analyzed on the binding of the closely related inhibitors. We present the crystal structures of the inhibitor complexes obtained by co-crystallizing an "intermediate" trypsin mutant. They could be determined to a resolution of up to 1.2 Å, and we measured the inhibitory activity (K_i) of each ligand against factor Xa, trypsin, and the various mutants. From these data we were able to derive a detailed structure–activity relationship which demonstrates the importance of aromatic interactions in protein–ligand recognition and their role in modulating enzyme selectivity. Pronounced preference is experienced to accommodate the benzamidine anchor with meta *topology in the S_1 specificity pocket. One ligand possessing only* para *topology deviates strongly from the other members of the series and adopts a distinct binding mode addressing the S_1' site instead of the distal S_3/S_4 binding pocket.*

Introduction

Factor Xa belongs to the class of serine proteinases, a family whose members share high similarity in the binding pocket and catalyze the same type of reaction; nevertheless they can selectively discriminate among specific substrates and inhibitors.[1] A large amount of structural data, determined by crystal structure analysis,[2] is available on factor Xa–ligand complexes, which has delineated the essential structural features dominating the inhibitor–factor Xa interactions. In particular, three major regions of the factor Xa active site have been identified as relevant for binding of high-affinity and selective ligands[2–7] (Figure 1): 1) the S_1 pocket, a narrow cleft with planar hydrophobic walls and a negatively charged Asp 189 at the bottom of the pocket that engages in a salt bridge with a positively charged lysine or arginine side chain of the substrate (P_1 residue); 2) the S_3/S_4 pocket, a surface-exposed cleft with hydrophobic residues at the floor (Trp 215) and walls (Tyr 99 and Phe 174); and 3) an electrophilic "cation hole", distal to S_3/S_4, formed by the carbonyl oxygen atoms of Glu 97, Thr 98, and Ile 175 that further stabilizes ligand positive charges in this region. Accordingly, most factor Xa inhibitors can be regarded as composed of three portions: the P_1 group which binds into the S_1 pocket, a linker or central scaffold designed to project attached substituents appropriately into the specificity pocket, and a remote group which interacts with the S_3/S_4 pocket and the distal "cation hole". The S_3/S_4 pocket usually accommodates a hydrophobic residue; it has been recognized however that the aromatic side chains of Phe, Tyr, and Trp possess a quadrupole moment and can participate in favourable interactions with a positive charge.[8,9] A survey[10] of the protein data bank (PDB) indicates that about 25% of all tryptophan residues experience an energetically significant cation–π interaction. It has been found that the S_3/S_4 sub-site of factor Xa provides an arrangement well-suited to form π–cation interactions. In additional studies, some interesting features have emerged leading to the general observation that factor Xa favours ligands with large hydrophobic substituents in the S_3/S_4 pocket.[4,6,7] This was also highlighted by a 3D QSAR study on serine proteinases:[11] the field contribution maps for hydrophobic properties indicate areas where increasing hydrophobicity of the inhibitors enhance affinity towards trypsin and particularly factor Xa in the S_3/S_4 pocket. Especially for the latter enzyme, this pocket is suggested to favour binding of potent ligands possessing bulky aromatic moieties. In this context, it is noteworthy that other serine proteinases exhibit fewer aromatic residues in the S_3/S_4 pocket, and selectivity is believed to be promoted by interactions experienced and successfully exploited in this pocket. In the same study[10] the analysis of the contribution

[a] *Dr. A. Di Fenza,[+] Dr. A. Heine, Prof. G. Klebe*
Institute of Pharmaceutical Chemistry, University of Marburg
Marbacher Weg 6, 35032 Marburg (Germany)

[b] *Prof. Dr. U. Koert*
Department of Chemistry, University of Marburg
Hans-Meerwein-Straße, 35032 Marburg (Germany)

[+] *current address:*
Institute for Chemical and Physical Processes (IPCF)–CNR
Area della Ricerca di Pisa, Via G. Moruzzi 1, 56124 Pisa (Italy)

Supporting information for this article is available on the WWW under http://www.chemmedchem.org or from the author.

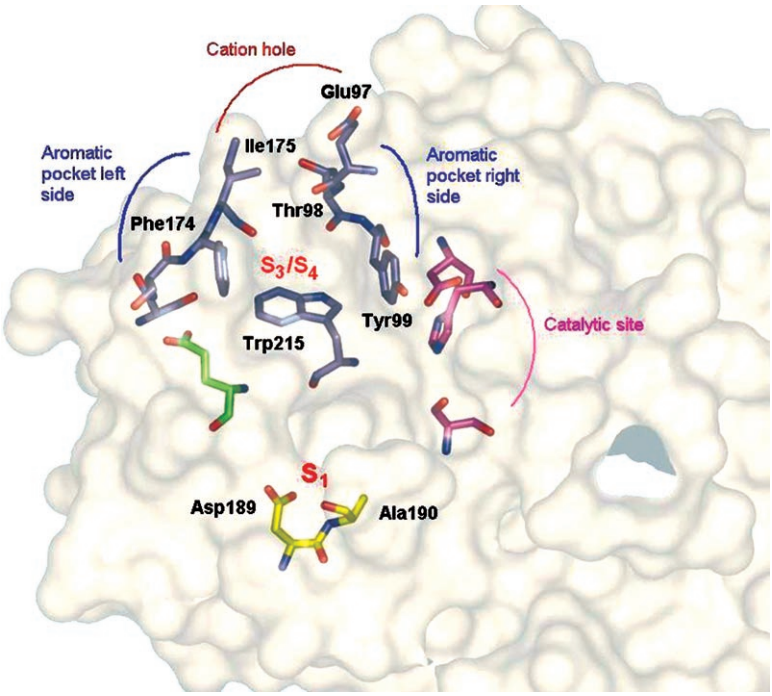

Figure 1. The binding pocket of factor Xa. A schematic decomposition of the binding site is shown, and the locations of the sub-sites S_1 and S_3/S_4 are indicated. The surface of the molecule is shown together with important residues coloured according to their atom type. Figure prepared using Pymol.[69]

maps resulting from hydrogen-bonding properties were less conclusive with respect to selectivity discriminating features among the inhibitors of serine proteinases.

In recent times, several development compounds have been described that bind into the S_1 specificity pocket of factor Xa exploiting uncharged groups such as a chlorobenzothiophene, chlorothiophene, or chloronaphthyl moiety.[2,5–7] These complexes suggest that formation of a favourable salt bridge via the basic group of a ligand with Asp 189 in the S_1 sub-site is not an absolute requirement for high-affinity binding to factor Xa.

Undoubtedly, aromatic interactions, usually described as π–π interactions, are ubiquitous in nature and are involved in many important biological processes.[12–15] For example, they are believed to provide stability to duplex DNA,[16] they have been proposed to contribute to the unique properties of thermophilic proteins,[17] and they may play a crucial role in aggregation of β-amyloid in Alzheimer's disease.[18] Aromatic interactions featuring tryptophan and tyrosine residues are prevalent in immunoglobulin antibodies with antigen-binding regions[19] and are found in excess in the groove of the major histocompatibility complex structure.[20] Similarly, the interactions between planar aromatic residues are important in stabilizing the tertiary structure of proteins.[21–23] Finally, the vast majority of drug molecules contain aromatic portions, and their differential recognition by proteins is likely dominated by aromatic–aromatic interactions.[24] In consequence, the pivotal role of non-covalent interactions involving aromatic rings for protein–ligand recognition and hence for drug design is an issue of current interest that needs to be further investigated.

The goal of this study is to analyse the role of the aromatic interactions to be experienced in the S_3/S_4 pocket of factor Xa with respect to the selectivity discrimination of this enzyme and related mutants versus four closely related inhibitors. Here, we investigated the interaction of these ligands towards recombinant protein mutants of trypsin which possess a hybrid binding pocket between trypsin and factor Xa.

The construction of factor Xa–trypsin hybrids has been reported elsewhere:[25,26] both the rat and bovine trypsin have been used as a starting point for site-directed mutagenesis to produce the stepwise transfer of the factor Xa binding site into trypsin. The mutants obtained were characterized by crystal structure analysis and enzyme kinetics with respect to the binding of different inhibitors.[27,28] These data indicate pronounced features, such as the structural reorganization of the binding site upon inhibitor binding. However, it is difficult to extract a simple and conclusive picture facing the selectivity profiles of the enzymes studied. This complexity is caused by the fact that the inhibitors of the series were structurally scarcely related. The compounds selected for the present study share an isosorbide moiety in common (one *exo*, one *endo* substituent as rigid central scaffold) to which benzamidino substituents P_1 and P_4 are attached with the polar groups in the *para* or *meta* positions. This results in several different combinations (Figure 2). Within such a closely related series of molecules only the characteristics about the stereochemistry should matter and determine the placement of either one of the *meta* or *para* attached amidino substituents, preferentially to the S_1 or S_4 site. This allows us to carry out a comparative analysis of the geometry of the aromatic interactions eventually involved in the S_4 aromatic pocket with respect to both the ligand and the binding-site geometry.

Results

Selection of the variants

Among the factor Xa–trypsin mutants mentioned above, we selected two mutants for our study which we believed to enhance the difference in binding of the inhibitors with respect to selectivity (Figure 3). Particularly, we considered the Asn 97 Glu and Leu 99 Tyr trypsin mutant, where Asn 97 and Leu 99 of trypsin are mutated to the corresponding residues in

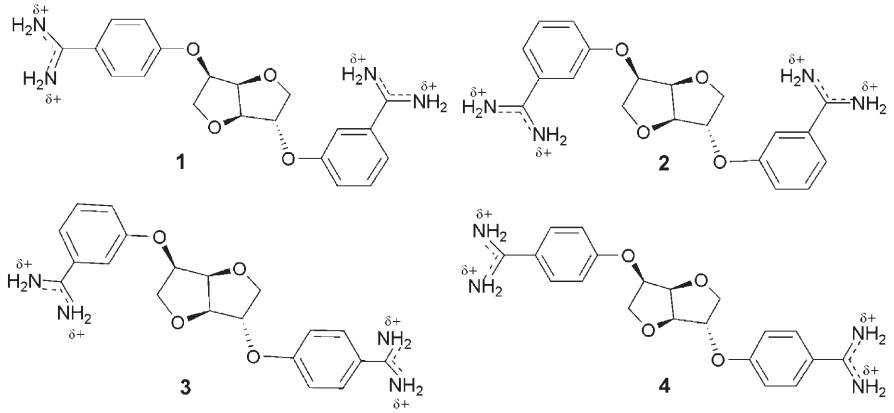

Figure 2. Chemical formulae of the ligands **1**–**4**.

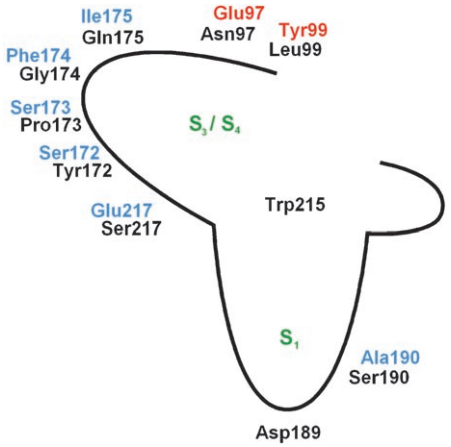

Figure 3. Schematic representation of the binding pocket of trypsin (black); point mutations performed to produce the 99XbT variant are indicated in red; additional mutagenesis to reveal the X(triple)GlubT variant are shown in blue. The latter mutant exhibits identical binding-site residue composition as factor Xa.

factor Xa.[29] These mutations introduce the correct aromatic wall (Tyr 99) of factor Xa into trypsin, so that the generated 99XbT mutant exhibits "partially" the aromatic S_3/S_4 binding sub-site of factor Xa. A second hybrid is realized by adding further mutations: Tyr 172 Ser, Pro 173 Ser, Gly 174 Phe, and Gln 175 Ile, which create the 175 loop of factor Xa in trypsin and produce the correct opposing aromatic wall of S_3/S_4: the Ser 190 exchange to Ala, which is positioned at the floor of the specificity pocket S_1 and Ser 217 Glu, which involves a residue that was shown to have a stabilizing effect on the 175 loop. This second mutant is termed the X(triple)GlubT mutant herein and it contains almost the entire binding site of factor Xa. Together with Trp 215, which is shared in common between trypsin and factor Xa, the binding site of this mutant provides now the complete aromatic box that is characteristic for the S_3/S_4 pocket in factor Xa.

Data set of ligands studied

The four ligands used in this study have been shown to be potent and selective factor Xa inhibitors.[30] They are characterized by a common dianhydrosugar isosorbide scaffold (one *exo*, one *endo*), a lead skeleton that has the advantage of combining high rigidity with stereochemical multiplicity. The different inhibitors were obtained by decorating the central scaffold with *para*- and *meta*-benzamidino substituents. In particular, ligands **1** and **3** exhibit a *para*-benzamidine and a *meta*-benzamidine in an exchanged substitution pattern with respect to the exocyclic oxygen atoms. Ligand **2** possesses both the benzamidino substituents in *meta*, while **4** holds both the amidino groups in *para* geometry (Figure 2).

Crystal structures of the variants

We determined the crystal structures of the 99XbT mutant in complex with all four stereoisomers. Well-diffracting crystals of all four complexes were obtained by co-crystallization techniques, all adopting the same crystal form (Table 1). In some cases, the inhibitor molecule contributes to crystal contacts as discussed further below. The binding geometry of all bound ligands is described by a well-defined electron density along with the interacting solvent molecules (Figure 4). In each complex, the overall structure of the trypsin mutant shows only minor perturbations with respect to the wild-type complexed by benzamidine (PDB code: 1C1N[31]), as quantified by rather low Cα atom rms deviations of 0.17, 0.16, 0.18, and 0.22 Å for the complexes with **1**, **2**, **3**, and **4**, respectively. The most pronounced differences occur upon binding of **4**, which deviates in its binding mode with respect to the other ligands, also indicated by the enhanced rmsd value of 0.22 Å (see below). All four inhibitors bind very similarly to the S_1 specificity pocket and form the expected amidine–carboxylate salt bridge at the bottom of S_1 thus exploiting one of the two benzamidine groups. It is interesting to note that ligands **1**, **2**, and **3** coordinate Asp 189 via a bidentate hydrogen bond through their *meta*-benzamidine substituents. Only **4**, which lacks a *meta*-benzamidine group, forms the bidentate hydrogen bond to Asp 189 with a *para*-substituted benzamidine. This indicated preference is in agreement with the observation that a benzamidine substituent at P_1 appears to be optimally suited for the geometry of the binding pocket, particularly if the binding topology with respect to the inhibitor's skeleton exhibits *meta* orientation.[2]

Crystal structure of 99XbT in complex with 1

In the crystal structure of the 99XbT mutant, ligand **1** wraps around Trp 215 with U-shape geometry: it inserts its *meta*-benzamidino group in the S_1 pocket, and the second *para*-benzamidine is placed in the S_3/S_4 pocket (see Figure S1 of Support-

Table 1. Data collection and refinement statistics.

	99XbT·**1**	99XbT·**2**	99XbT·**3**	99XbT·**4**
Resolution range [Å]	50.0–1.60	50.0–1.20	50.0–1.40	50.0–1.65
Space group	$P3_121$	$P3_121$	$P3_121$	$P3_121$
Unit cell [Å]	$a, b = 54.8, c = 108.6$	$a, b = 54.7, c = 108.0$	$a, b = 54.8, c = 108.6$	$a, b = 54.4, c = 105.1$
Highest resolution shell [Å]	1.60–1.63	1.20–1.22	1.40–1.42	1.65–1.68
No. of observations	120449	276813	208808	90584
No. of unique reflections	46808	107803	71411	38788
Completeness [%]	97.2 (90.1)[a]	95.5 (68.8)[a]	99.4 (94.6)[a]	92.7 (55.4)[a]
Mean I/σ	18.2 (1.9)[a]	18.9 (1.6)[a]	18.6 (2.0)[a]	14.3 (2.2)[a]
R_{sym} [%][b]	5.2 (44.4)[a]	4.6 (45.4)[a]	5.5 (42.0)[a]	7.5 (28.2)[a]
Refined residues	223	223	223	223
Refined water molecules	227	249	242	233
Refined ligand atoms	28	28	28	28
Refined ions	$1\,Ca^{2+}$, $2\,SO_4^{2-}$	$1\,Ca^{2+}$, $1\,SO_4^{2-}$	$1\,Ca^{2+}$, $1\,SO_4^{2-}$	$1\,Ca^{2+}$, $2\,SO_4^{2-}$
R_{cryst} ($F_o > 4\sigma F_o$; F_o)[c]	14.3; 15.7	11.2; 12.3	14.9; 16.3	15.4; 16.0
R_{free} ($F_o > 4\sigma F_o$; F_o)[d]	19.7; 21.5	15.2; 16.7	19.2; 21.1	20.9; 22.1
		Rms deviations		
Bond lengths [Å]	0.008	0.013	0.010	0.007
Bond angles [°]	2.1	2.3	2.4	2.0
Average B value [Å^2]	17.9	16.8	15.4	21.7
Main chain	19.9	13.1	11.6	18.6
Side chain	17.9	16.2	15.4	22.3
Ligand	25.6	23.7	18.4	22.9
Waters	29.2	29.5	27.1	30.0
		Ramachandran plot[e]		
Most favoured [%]	88.3	89.4	88.8	87.8
Additional allowed [%]	11.7	10.6	11.2	12.2
Generously allowed [%]	0	0	0	0
Disallowed [%]	0	0	0	0

[a] Values in parentheses are statistics for the highest resolution shell. [b] $R_{sym} = [\Sigma_h\Sigma_i | I_i(h) - \langle I(h)\rangle | / \Sigma_h\Sigma_i I_i(h)] \times 100$, where $\langle I(h)\rangle$ is the mean of the $I(h)$ observation of reflection h. [c] $R_{cryst} = \Sigma_{hkl} | F_o - F_c | / \Sigma_{hkl} | F_o$. [d] R_{free} was calculated as for R_{cryst} but on 5% of the data excluded from the refinement. [e] From Procheck.[76]

ing Information). At the bottom of the S_1 pocket the *meta*-amidine group forms a bidentate salt bridge with the carboxylate group of Asp189, showing mutual O–N distances of 2.9 and 2.8 Å, respectively (Figure 5). The NH_2 group, involved in the longer H-bond to one of the carboxylate oxygen atoms of Asp189, forms three additional H-bonds: one to the carbonyl oxygen atom of Gly219, a second, mediated by a water molecule to the hydroxy oxygen atom of Tyr172, and a third to the carbonyl oxygen atom of Ser190. The interstitial water molecule is conserved among all structures with a *meta*-benzamidino substituent in S_1 but it is missing in the complex with the exclusively *para*-substituted inhibitor **4**. The second NH_2 group, involved in the shorter H-bond, binds, in addition to the second carboxylate oxygen atom of Asp189, to Oγ and the backbone carbonyl oxygen atom of Ser190. Furthermore, a buried water molecule mediates an interaction to the carbonyl oxygen of Val227. The interactions of this NH_2 group are conserved across all four structures and have also been observed in other crystal structures of trypsin in complex with benzamidine-type inhibitors.[4,5] A sulfate ion, frequently observed in trypsin structures, is present in the vicinity of the specificity pocket. It coordinates to Oγ of Ser195 (2.6 Å, 3.0 Å), to NH of Gly193 (3.1 Å), to Nε2 of His57 (2.8 Å), and, in the complex with **1**, via a water molecule to one of the endocyclic oxygen atoms of the ligand's sugar scaffold (2.6 Å) and to OH of Tyr99 (2.6 Å) (data not shown). Also one of the exocyclic ether oxygen atoms of **1** is involved in an H-bond to a water molecule (Figure 5). Except for the latter two H-bonds to water molecules, the sugar scaffold does not penetrate significantly into the S_3/S_4 pocket; accordingly it does not seem to be involved in any further polar or hydrophobic interactions. The S_3/S_4 pocket is mainly occupied by the *para*-benzamidino group in such a way that its phenyl moiety most likely experiences distinct edge-to-face interactions with the side chains of Tyr99 and Trp215. In particular, the angle between the planes passing through the Tyr99 phenyl moiety and the *para*-benzamidine of **1** is 123.8°, while the angle between the planes passing through the *para*-benzamidine of **1** and the Trp215 indole is 150.5°; the distance between the centroids of the Tyr99 phenyl and the benzene ring of *para*-benzamidine of **1** (as defined by the centroids of their corresponding benzene rings) is 4.5 Å (see Table ST1 and Figure S2 of Supporting Information for explanation), while the distance between the centroids of the benzene ring of Trp215 and that of the *para*-benzamidine of **1** is 4.7 Å (see Table ST1 and Figure S2 of Supporting Information for explanation). In this orientation the rim-exposed C–

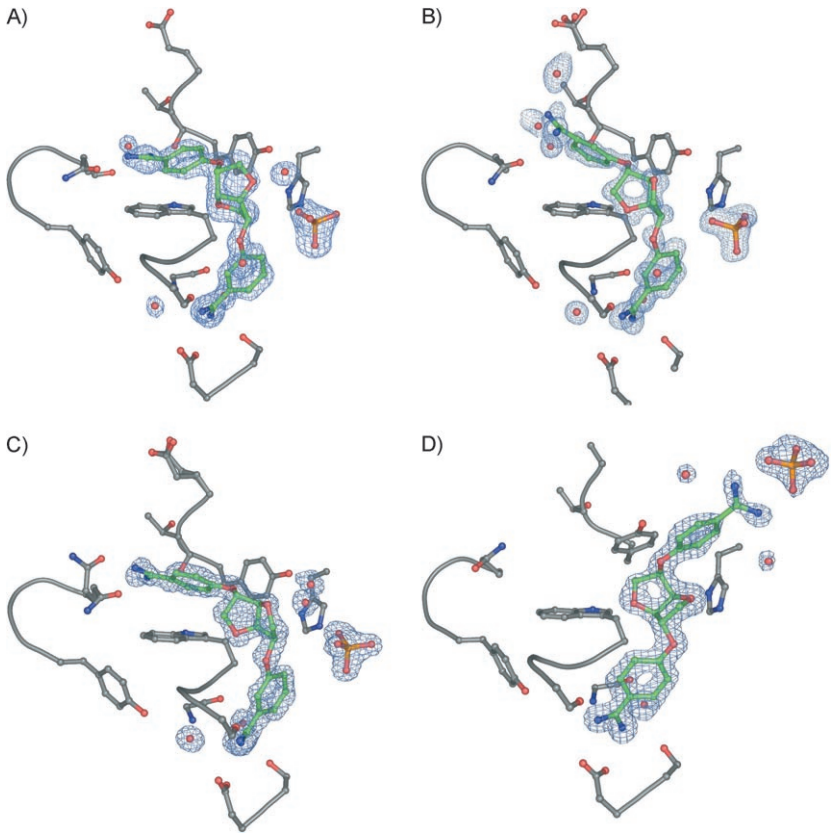

Figure 4. View of the 99XbT mutant complexed to **1** (A), **2** (B), **3** (C), and **4** (D), with the F_o–F_c electron density (at a σ level of 1.5) shown in light blue, encompassing the ligand molecules (in green), water molecules (in red), and the sulfate ion (in orange).

H bonds of the positively charged *para*-benzamidine moiety interact with the electron-rich centres of the phenyl (Tyr 99) and indole moiety (Trp 215) (Figure 6).

In the "cation hole", one of the amidino nitrogen atoms forms H-bonds to the carbonyl oxygen atom of Thr 98 and via a stable water molecule (B-factor: 22.4) to the carbonyl oxygen atom of Gln 175, whereas the second NH_2 group is hydrogen-bonded to the Oε1 atom of Gln 175. In the crystal structure, this NH_2 group is in further contact to Oγ of Ser 127 of a symmetry-related protein molecule (Figure 5).

In addition to the above-described interactions, the ligand establishes in total 81 van der Waals contacts and its surface becomes buried to 76.5% by the closest neighbouring protein molecule. Including entries of the crystal packing 92 contacts are formed and 97.4% are buried.

Crystal structure of 99XbT in complex with 2 and 3

Since the structures of **2** and **3** superimpose nearly identically except for the distal amidino group, their binding modes are described together. The two inhibitors bind to the S_1 site quite identically with respect to each other and very similarly to ligand **1**. Via the *meta*-benzamidine moiety, they form, in addition to the bidentate salt bridge to Asp 189 (2.9 and 2.8 Å for **3**; 3.0 and 2.9 Å for **2**), six similar hydrogen bonds. The first NH_2 group is involved in the longer H-bond to one of the carboxylate oxygen atoms of Asp 189. Furthermore, it interacts with the carbonyl oxygen atom of Gly 219 (2.9 Å for **3**; 2.8 Å for **2**), a contact to the terminal OH of Tyr 172 is mediated via a water molecule (3.1-H_2O-3.4 Å for **3**; 3.0-H_2O-3.3 Å for **2**), and the carbonyl oxygen atom of Ser 190 binds to both NH_2 groups. The second NH_2 forms H-bonds to Oγ of Ser 190 (3.1 Å for **3**; 3.0 Å for **2**) and to the carbonyl oxygen of Val 227 via an interstitial water molecule (3.0-H_2O-2.8 Å for **3**; 2.9-H_2O-2.4 Å for **2**; Figure S1 (Supporting Information) and Figure 5).

Both ligands **2** and **3** place their central sugar scaffold with exactly the same orientation into the binding pocket, nevertheless slightly different interactions are observed for contacts mediated by solvent molecules: **2** forms an H-bond via its exocyclic ether oxygen to a water molecule (3.2 Å) similarly to **1** (2.9 Å), while **3** binds with one of its endocyclic oxygen atoms to the OH group of Tyr 99 via a chain of two mediating water molecules (Figure 5) and to a further symmetry-related water molecule (2.7 Å). Finally, both ligands bind to the Gly 216 NH in the protein backbone via the second endocyclic oxygen (3.4 Å for **3** and 3.3 Å for **2**).

Similarly to **1**, also **2** and **3** wrap around Trp 215 and accommodate the S_3/S_4 pocket with their *meta*- or *para*-benzamidino moieties, respectively. Both ligands place their phenyl moiety of the distal benzamidino substituent with respect to the indole moiety of Trp 215 in a way that aromatic interactions are formed (Figure 6). The benzene rings of **2** and **3** deviate from parallel stacking with that of Trp 215 by angles of 36.2° and 24.4°, respectively, measured between best planes through both moieties. The distance between the centroids of the latter groups amounts to 4.2 and 4.4 Å, respectively (see Table ST1 and Figure S2 of Supporting Information). Furthermore, the benzamidino groups of **2** and **3** are arranged in edge-to-face geometry towards the phenyl moiety of Tyr 99. The angle between best planes through the two aromatic moieties is 57.5° for **2** and 60.1° for **3.** The distance of the centroids is 4.8 Å for **2** and 4.9 Å for **3** (Table ST1 of Supporting Information).

In **3**, the distal *para*-benzamidine falls exactly between the carbonyl oxygen atom of Thr 98 and Oε1 of Gln 175, forming H-bonds to these residues (2.9 Å to Thr 98 and 3.4 Å to Gln 175 with one NH_2 group; 2.5 Å to Gln 175 with the other NH_2

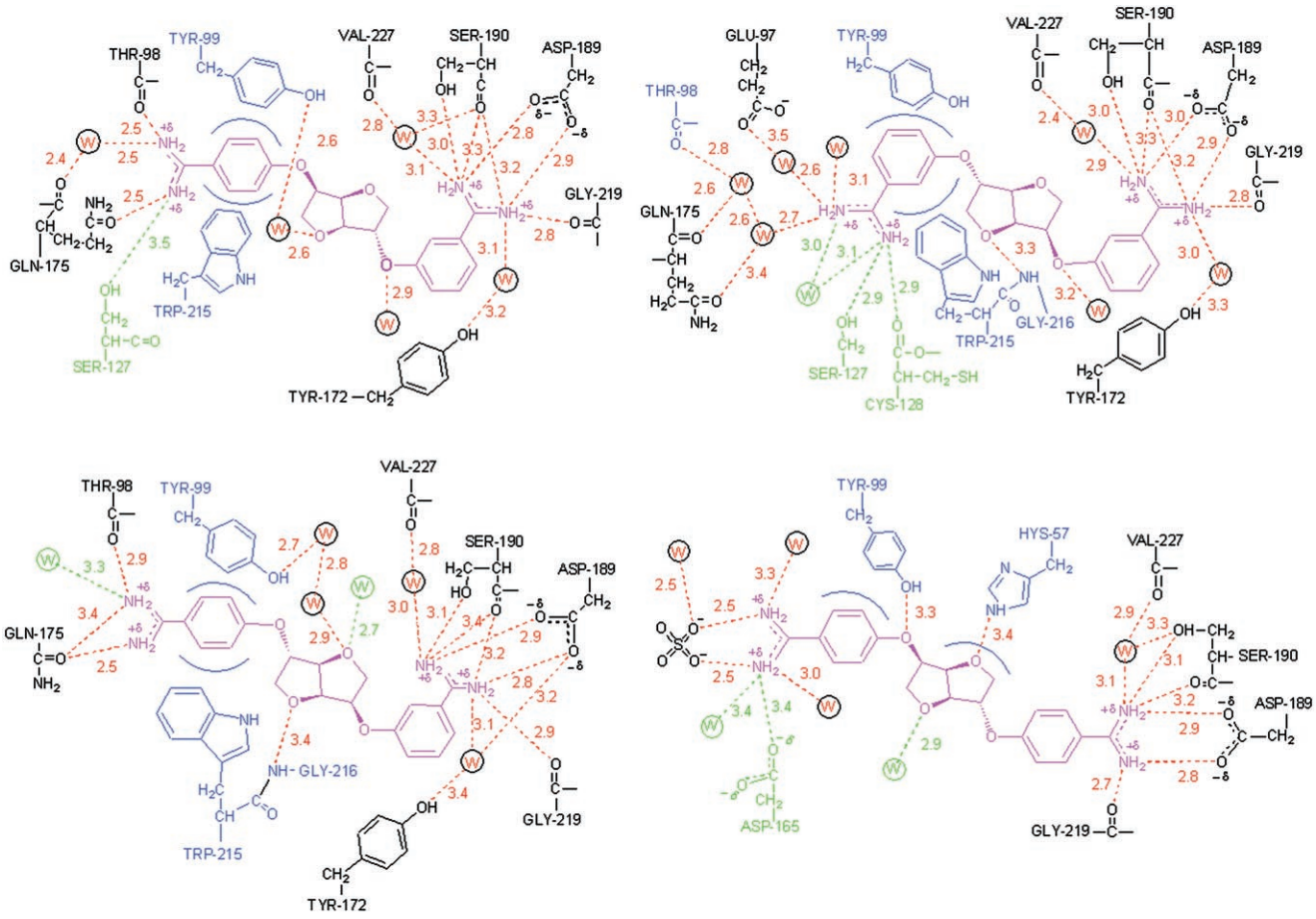

Figure 5. Schematic drawing of the interactions formed between the 99XbT mutant and **1** (upper left), **2** (upper right), **3** (lower left), and **4** (lower right). Hydrogen bonds are shown as red dotted lines, and the residues that interact with the ligand via a polar group are coloured in black. Aromatic and hydrophobic residues with a distance less than 5 Å around the inhibitors are coloured in blue. Symmetry-related residues or water molecules in contact with the ligand are indicated in green. H-bond lengths are given in Å.

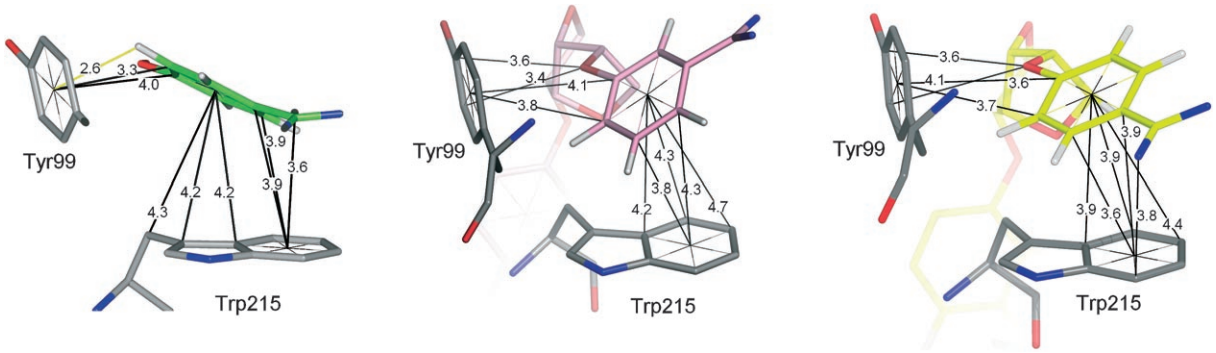

Figure 6. Aromatic–aromatic interactions formed between the phenyl moiety of the distal benzamidino group of **1** (green), **2** (pink), and **3** (yellow) and the residues Tyr 99 and Trp 215 in the S_3/S_4 pocket of 99XbT; black lines indicate aromatic contacts, and in yellow short CH–aromatic ring contacts are shown. All distances are given in Å.

group) and to a symmetry-related water molecule (3.3 Å). In contrast, the distal *meta*-benzamidino moiety of **2** orients towards Gln 175 and only one of its NH_2 groups is engaged in an H-bond to the protein mediated via water molecules. It binds through a water molecule (B-factor 50.0) to Oε1 of Glu 97 and via a network of two water molecules (B-factors: 18.2 and 37.1) to both carbonyl oxygen atoms of Gln 175 (Figure 5). Furthermore, it is in contact with a symmetry-related water molecule (3.0 Å). The second NH_2 function forms hydrogen bonds to Oγ of Ser 127 and the carbonyl oxygen of Cys 128 (both 2.9 Å) of a

symmetry-related protein molecule in the crystal packing. Additionally, it shares interactions to the symmetry-related water molecule with the former NH_2 group (3.1 Å) (Figure 5).

In both complexes, similar to that with **1**, a conserved sulfate ion is observed in the neighbourhood of the specificity pocket which is coordinated to Ser195Oγ, Gly193NH, and His57Nε2 (data not shown).

The total number of van der Waals contacts experienced by **2** and **3** is 78 (89 in the packing) and 94 (100 in the packing), respectively. Both ligands bury 72.2% (**2**, 97.2% in the packing) and 80.0% (**3**, 99.5% in the packing) of their surfaces by contacts with the protein.

Crystal structure of 99XbT in complex with 4

With respect to the other ligands, inhibitor **4** binds in a completely different orientation (Figure S1 of Supporting Information and Figure 5). Lacking *meta* topology, it has to interact via a *para*-benzamidino group with the S_1 pocket, and the remaining part of the molecule is found in an extended conformation, pointing away from the S_3/S_4 binding pocket. The interactions experienced in the S_1 site are similar to those found for the ligands **1**, **2**, and **3**: a salt bridge to Asp189 (2.9 and 2.8 Å) and additional H-bonds to the carbonyl oxygen atom of Gly219 (2.7 Å); nevertheless, the conserved water molecule, which mediates binding to the Tyr172 hydroxy oxygen atom in the other structures, is missing. Further H-bonds are formed to Oγ and the carbonyl oxygen of Ser190 (3.2 Å and 3.1 Å, respectively) and to the carbonyl oxygen atom of Val227 which is mediated via a water molecule (Figure 5).

The sugar scaffold of **4** orients, in contrast to the other ligands, not towards the S_3/S_4 pocket, but is placed between the side chains of Tyr99 and His57. Interestingly, as a consequence the Tyr99 side chain is rotated by 90° with respect to its orientation in the other three structures, towards the interior of the active site. This rearrangement of the Tyr99 side chain creates a new hydrophobic pouch which allows accommodation of the dianhydrohexitole moiety of the sugar backbone through hydrophobic interactions with the protein (Figure 7). In particular, two carbon atoms of the isosorbide, which are partially positively polarized due to their close proximity to oxygen atoms, are in a position that likely allows them to interact with the electron-rich centre of the phenyl moiety of Tyr99. This effect adds to the attraction exerted from the phenolic OH group of Tyr99 which faces the two isosorbide carbon atoms. Via one of the endocyclic oxygen atoms, the sugar scaffold is also involved in an H-bond to a symmetry-related water molecule (2.9 Å). The other distal *para*-benzamidine group forms a salt bridge via its amidino nitrogens to two oxygen atoms of a sulfate ion (Figure 5). In addition, each NH_2 group H-bonds to water molecules (3.0, 3.3, and 3.4 Å), and one of them results from a symmetry-related contact. A further interaction is formed to Oδ of the symmetry-related Asp165 (3.4 Å). Besides the ligand, the sulfate ion coordinates to a water molecule (2.5 Å), however, it does not make any further interactions to the protein in contrast to the other complexes with the previous ligands (Figure S1, Supporting Information). Interestingly, the sulfate ion resides outside the binding pocket just as if it had been pushed off from its frequently observed location in other structures (close to the catalytic triad) to compensate locally the positive charge on the second amidino groups of the ligand. The latter accommodates in the interstitial space left unoccupied in the crystal packing and it forms contacts to a symmetry-related protein molecule (Figure 8).

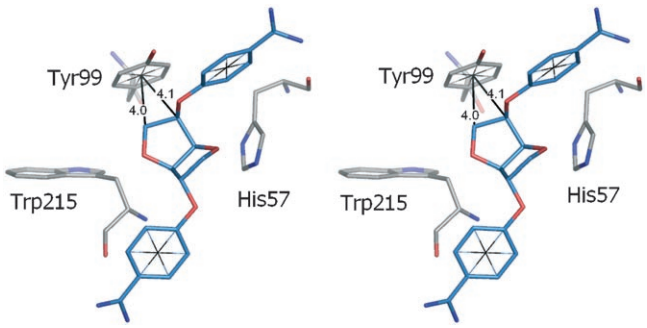

Figure 7. Stereo image showing intermolecular aromatic contacts of the central sugar moiety of **4** (blue) with the rearranged residue Tyr99 and His57 in the complex with 99XbT (grey). All distances are given in Å.

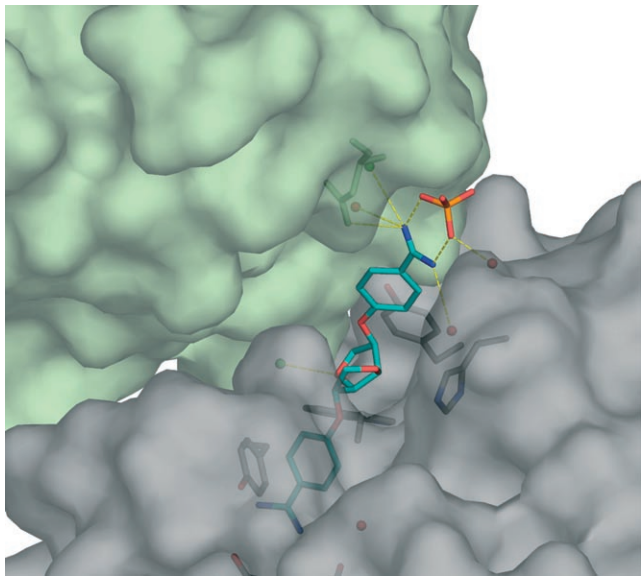

Figure 8. Accommodation of **4** in the crystal packing of the 99XbT mutant. Two symmetry-related protein molecules (grey, green) are shown with transparent molecular surface. Ligand-contacting residues and water molecules are indicated (hydrogen bonds as yellow dashed lines).

The total number of van der Waals contacts formed by **4** with the protein amounts to 70 (77 in the packing), and 65.9% (92.1% in the packing) of the ligand's surface area is buried by the protein.

Binding analysis of the variants

K_i values were determined for all four inhibitors **1**–**4** with respect to human factor Xa, the X(triple)GlubT mutant, the

99XbT mutant, and bovine trypsin (Table 2). Among the ligands studied, **1** possesses the highest inhibitory activity against all chimeric enzymes analysed. It is interesting to note that the inhibitory activity of **1** increases while proceeding from trypsin

Table 2. Binding constants for the inhibition of human factor Xa, bovine trypsin, and two trypsin mutants.

	K_i [μM][a]			
Ligand	Factor Xa	X(triple)GlubT	99XbT	b-Trypsin
1	0.02 ± 0.00	0.03 ± 0.00	0.22 ± 0.06	0.43 ± 0.06
2	0.73 ± 0.21	0.53 ± 0.04	1.19 ± 0.17	1.81 ± 0.51
3	1.15 ± 0.31	0.73 ± 0.02	1.33 ± 0.28	1.51 ± 0.24
4	4.28 ± 0.90	0.62 ± 0.02	1.26 ± 0.18	1.20 ± 0.22

[a] K_i values were measured in triplicate according to the method of Dixon,[75] using the substrate Pefachrome-tPA (405 nm) at 25 °C in 50 mM Tris-HCl (pH 8), 154 mM NaCl, 5% EtOH, and 10 mM $CaCl_2$.

to the factor Xa binding site. The three remaining ligands (**2**, **3**, **4**) exhibit equivalent inhibitory potency against all proteins. Ligands **2**, **3**, and **4** show approximately the same K_i values for the wild-type bovine trypsin and the 99XbT mutant. However, for the X(triple)GlubT mutant the inhibitory potency increases by a factor of 2 for ligands **3** and **4** and a factor of 3 for ligand **2** compared to the bovine trypsin wild-type. Interestingly, ligands **3**–**4** show no significantly increased selectivity for factor Xa, while **2** binds somewhat stronger to factor Xa. Ligand **4** even loses affinity for factor Xa and is therefore a sixfold weaker inhibitor towards factor Xa compared to the triple mutant (Table 2).

Discussion

The analysis shows that **4** adopts a completely different binding mode compared to the remaining derivatives, except for the contacts formed in the S_1 sub-site which are quite similar in all cases. In the latter pocket the only exception is observed for **4** where a conserved water molecule is missing that usually mediates the binding of factor Xa-specific inhibitors to Tyr 172. Apart from the S_1 pocket, **4** behaves very different from the other ligands and many typical factor Xa or trypsin inhibitors.[7–10] Across our series, **4** is the only ligand that has to place a *para*-benzamidino functionality in the S_1 pocket, whereas the other inhibitors can use their *meta*-benzamidino substituents for the interactions in S_1. This probably explains the distinct binding mode of **4** that, due to its deviating chemical topology, has no other option to bind. In particular, **4** does not adopt a kinked overall conformation, required to follow the binding-site architecture in the trypsin-like serine protease family. Instead it retains an extended geometry and it places its distal benzamidino function away from the binding site towards P_1' and close to neighboring protein molecules in the crystal packing (Figure 8).

It is very difficult to assess whether the binding mode of **4** observed in our crystal structure also represents the situation under the conditions used to determine the binding constants. In the crystal structure, the ligand orients towards the P1′ site simultaneously inducing a pronounced conformational adaptation of Tyr 99. The aromatic side chain of this residue forms, together with the imidazole moiety of His 57, a hydrophobic crevice that accommodates the sugar skeleton of **4** together with part of the distal benzamidino substituent. The S_3/S_4 pocket and the cation hole remain virtually unoccupied. Ligand **4** appears to be the weakest binder of the series, in particular towards factor Xa, however, the drop in affinity is only marginal. In case the observed binding mode is also relevant under the applied assay conditions, the affinity collected by binding in this alternative fashion seems to be quite similar to that experienced by the other three ligands.

The closely related binding modes of **1**, **2**, and **3** permit a more detailed comparison. All ligands address the cation hole and experience contacts to the same residues. However, **2** uses several water molecules to mediate binding, whereas the other two perform direct interactions (**3**) or involve one further water molecule (**1**, Figure 5). With respect to the central dianhydrohexitole scaffold, **2** and **3** adopt virtually identical binding modes (Figure 9). The sugar moiety adopts a bowl-

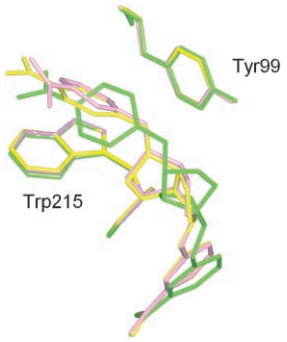

Figure 9. Superposition of **1** (green), **2** (pink), and **3** (yellow) and the corresponding binding site (only two residues are depicted for clarity) of the 99XbT mutant.

shaped geometry and enables the kinked overall structure of the ligands. In **2** and **3** it orients its convex face towards the Tyr 99 rim of the binding pocket. Due to inverted stereochemistry, the sugar portion of **1** occupies a slightly different position in the binding pocket and exposes its convex face to the opposite side. This small translation of the dianhydrohexitole in **1** compared to **2** and **3** places the phenyl moiety of the distal benzamidino substituent well in front of the aromatic ring of Tyr 99. As **2** and **3** penetrate deeper into the S_3/S_4 pocket, the placement of their corresponding phenyl rings results in less pronounced contacts with the aromatic portion of Tyr 99. Furthermore, the phenyl ring in **1** is inclined to the opposite direction compared to **2** and **3** (Figure 9). Analysis of the aromatic contacts formed by **1**, **2**, and **3** with Tyr 99 and Trp 215 shows qualitative differences which are difficult to translate into quantitative binding contributions. One important feature of aromatic interactions is their directionality. The electrostatic model proposed by Hunter and Sanders[32,33] assigns a quadrupole moment to the phenyl moieties and bond

dipoles along the C–H bond vectors. This charge distribution reinforces the mutual packing of aromatic rings, resulting in perpendicular T-shaped edge-to-face arrangements. However, with reduced influence of the C–H bond dipoles, parallel stacking is increasingly adopted. Both geometries are of deviating strength and represent in a particular structure the best compromise between attractive and repulsive interactions. Theoretical and experimental studies[34–42] on the packing of aromatic molecules such as benzene, toluene, s-tetrazine dimers, and other heterodimers revealed that the T-shaped geometry represents a preferred arrangement of the benzene dimer in the gas-phase[43,44] as well as in the liquid phase.[45] In the crystalline state, a distance of approximately 5 Å between the ring centres is found.[46–49] Furthermore, the analyses of the interaction geometry of aromatic side chain residues in proteins and protein complexes have been performed[15,50–53] and underline that there is no pronounced preference for one particular arrangement. Obviously, a competition between stacked and T-shaped geometry is given; which one prevails depends on the distance between the aromatic rings, the type of ring substituents, and the local environment (for example, interacting protein or solvent environment).

In the crystalline complex, **1** adopts an edge-to-face arrangement with CH–π interactions between the distal benzamidine group and the protein residues Tyr 99 and Trp 215 in the S_3/S_4 pocket (Figure 6 and Table ST1, Supporting Information). Ligands **2** and **3** have their distal benzamidino moieties rotated by $\approx 90^\circ$ compared to **1**. In this way, the geometry to the aromatic portion of Tyr 99 and Trp 215 is again edge-to-face but inverted with respect to Tyr 99 and Trp 215, and possibly explains the differences in affinity in respect to **1** (see Table ST1 and Figure S2 of Supporting Information).

These differences can be visualized using DrugScoreCSD.[54,55] This program evaluates knowledge-based pair potentials to energetically ranked non-bonded contact interactions. Through the evaluation of occurrence frequencies of short contacts in small-molecule crystal packings, statistical potentials have been derived. In Figure 10, the evaluation is displayed on a per-atom scale. The contribution of each atom to the total energy score is shown in terms of scaled and coloured spheres. The absolute value of the potential contribution relates to the radius of the sphere. Blue colours indicate attractive interactions and red, repulsive. In summary, for the aromatic moiety of **1** larger contributions are indicated as compared to **2** and **3**. For the latter, even one carbon experiences slightly repulsive scoring. This diagram shows very intuitively the differences in the aromatic interactions to binding for the three complexes. At this point, the question must be allowed, why **2**, exhibiting *meta-meta* stereochemistry, does not use its opposite aromatic face to occupy the S_1 pocket? This would allow **2** an identical binding mode to **1.** The latter inhibitor experiences, due to the better placement of its distal phenyl moiety in S_3/S_4, more favourable aromatic–aromatic interactions. Different from **1**, **2** would then show a *meta*-attached amidino group in S_3/S_4. This connectivity would create deviating interaction topology, and the above-described opposite ring inclination would be impossible as the *meta* attachment would clash for steric reasons with Trp 215. Obviously, the inventory of the different mutually competing interactions with respect to both possible binding modes of **2** favour the placement of the benzamidino group with stereochemistry as found in **3** into the S_1 pocket instead of that found in **1**.

Taking the affinity difference in the series of inhibitors with respect to trypsin, factor Xa, and the mutants into account, supposedly the binding pose of **1** results in best aromatic packing. For trypsin, where the S_3/S_4 pocket exhibits only one aromatic residue (Trp 215), a slight advantage is experienced. However, this advantage of **1** over **2** and **3** is enhanced when the more complete aromatic binding "box", as actually found in factor Xa, is established by the mutated proteases (Table 2). Once all three faces of the box are represented by aromatic residues (Trp 215, Tyr 99, Phe 174) as in factor Xa, the affinity improves by a factor of 25.

The predominant role of aromatic interactions in host–guest and protein–ligand complexes, which has been stressed in several case studies,[56–60] demonstrates the important role of these interactions for selectivity discrimination among ligands. Possibly, **1** is better suited to exploit an optimal aromatic packing present in factor Xa; in consequence it exhibits the most pronounced selectivity discrimination across the series of ligands.

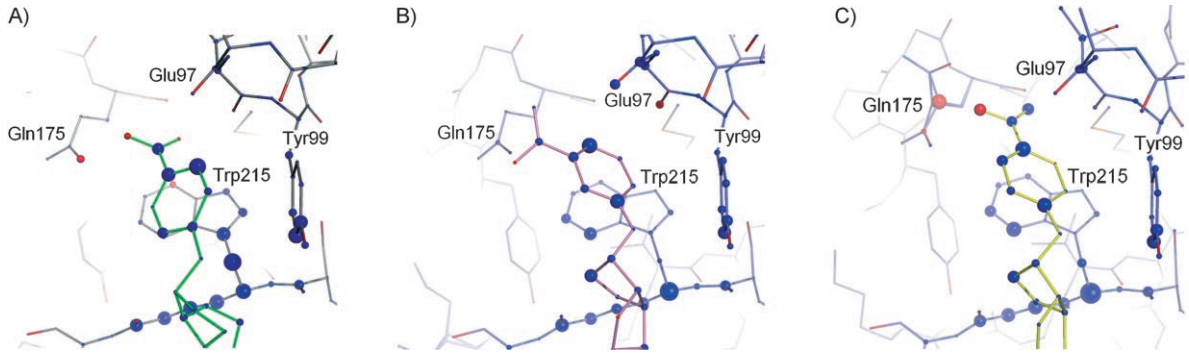

Figure 10. Visualization of the per-atom score contributions, derived by DrugScoreCSD[54,55] for the 99XbT mutant (grey) in the crystallographically determined binding mode of **1** (A), **2** (B), and **3** (C). Favourably interacting atoms are indicated as blue spheres; unfavourable ones in red. The size of the spheres scales with the absolute values of the per-atom score contribution.

Summary and Conclusions

Crystal structure analysis of four congeneric bis-benzamidino dianhydrosugar isosorbide ligands with an Asn 97 Glu, Leu 99 Tyr mutant of bovine trypsin suggests preferred binding of the benzamidine anchor with *meta* topology in the S_1 pocket. In all examples with the latter topology a related binding mode is found. Only ligand **4** exhibiting both benzamidino groups in *para* position adopts a strongly deviating non-customary binding mode. It induces pronounced induced-fit adaptations of the protein. A small hydrophobic crevice opens up flanked by the rearranged Tyr 99 and His 57. It subsequently hosts the hydrophobic sugar portion of the ligand (Figure 7). The second benzamidine moiety orients towards the P_1' site leaving the S_3/S_4 pocket virtually unoccupied. The remaining ligands **1**, **2**, and **3** show similar binding modes. Their *meta* benzamidino groups occupy the S_1 pocket with nearly identical geometry in all three cases. The second benzamidino moiety, present with either *meta* or *para* topology is hosted in the remote part of the S_3/S_4 pocket. The three structures differ in this region by a deviating network of water molecules mediating interactions between the ligands and the chimeric enzyme. Obviously, the water molecules serve as versatile space holders and buffer for promiscuous recognition of different functional groups attached to the dianhydrohexitole skeleton in this region.

The deviating stereochemistry of the central sugar scaffold and the substitution pattern of the distal benzamidine moiety have an influence on the placement of the aromatic ligand portion in the S_3/S_4 pocket. This latter pocket shows increasing aromatic character proceeding from trypsin (only Trp 215) to factor Xa (Trp 215, Tyr 99, Phe 174) via our chimeric mutants. Accordingly, the establishment of favourable directional aromatic–aromatic interactions in this pocket with a bound ligand will increasingly contribute to binding affinity and will thus determine selectivity.

Due to the above-mentioned stereochemical differences, **2** and **3** penetrate deeper into the S_3/S_4 pocket compared to **1**. In consequence, the two former ligands place the phenyl moiety of their distal benzamidino group in a less pronounced contact with the aromatic portions of Tyr 99 and Trp 215. In contrast, **1** seems to achieve an ideal placement of its phenyl ring well in front of Tyr 99 and Trp 215. Interestingly enough, the inclination of the phenyl ring plane in **1** is opposite to that adopted by **2** and **3** in the protein complex. This again indicates better established directional aromatic–aromatic interactions with the aromatic recognition site of the protease. Assuming that the conserved binding mode of **2**, **3**, and **1** found for the X99bT mutant is also valid for factor Xa, the binding geometry provides an explanation why **1** exhibits the strongest selectivity discrimination between trypsin and factor Xa. As the latter inhibitor exploits best the directional interactions with the aromatic recognition site, it experiences most sensibly the gradual exchange of aromatic versus aliphatic residues in S_3/S_4. In trypsin, Leu 99 and the hydrophobic ethylene side chain of Gln 175 flank the S_3/S_4 pocket. The aliphatic character of these residues provoke much fewer directional interactions than the aromatic amino acids Tyr 99 and Phe 174 found at the same position in factor Xa.

We therefore conclude that factor Xa is more selective with respect to trypsin for ligands which opportunely interact with the fully established aromatic box in the S_3/S_4 sub-site. For this reason, studies aimed at the design of factor Xa-specific inhibitors should be tailored towards the synthesis of compounds possessing scaffolds characterized by the ability to promote aromatic interactions along with an appropriate packing geometry to favour them.

Experimental Section

Mutagenesis, expression, refolding, and purification of the mutants: The bovine trypsin mutated sequences were constructed by site-directed mutagenesis using the Quick-Change™ kit[61] and transformed in *E. coli* strain BL21(DE3)pLys. The proteins, obtained in the form of inclusion bodies, were purified and refolded as described.[26,62]

Crystallisation, data collection, and structure analysis: Crystals of the protein–inhibitor complexes were obtained by co-crystallisation. Each inhibitor was pre-incubated with the bovine β-trypsin partial mutant in 2 mM HCl and 10 mM $CaCl_2$ for 3–4 h at 4 °C. Co-crystallization was carried out at 20 °C by using vapour diffusion (hanging drop). Trigonal crystals grew, after few days, in 24–30 % PEG 8000, 0.1 M imidazole (pH 7) and 0.1–0.3 M ammonium sulfate at protein concentration of 20 mg mL^{-1} and about 10-fold inhibitor concentration.

The diffraction experiments for the complexes with the inhibitors **1**, **2**, and **3** were carried out at the Protein Structure Factory beamline BL14.1 of Free University Berlin at BESSY with data collected on a MAR-CCD detector (Marresearch, Norderstedt, Germany), while experimental data for the complex with **3** were collected in house, using a Rigaku R-axis IV++ image plate system (MSC, Texas, USA) installed on a Rigaku RU300 rotating anode generator. In all cases, the crystals were measured under cryo-conditions at −170 °C. Here, the crystallization buffer containing 25 % glycerol was used as cryoprotectant. The program HKL2000[63] was used for data processing and scaling, and the structure solutions were obtained by molecular replacement with the software AMoRE[64] from the package CCP4,[65] using starting coordinates taken from the Protein Data Bank (PDB code: 1MTV[5]).

Conventional crystallographic refinement (rigid body, positional, temperature factor, slow-cooling) was carried out for the first 3–4 cycles with CNS,[66] and for the remaining cycles refinement was continued with SHELXL-97.[67] Molecular models of the inhibitors were constructed using SYBYL (Tripos, Inc., St. Louis, MO, USA) and model building was performed using O.[68] Protein superpositions based on Cα atoms were obtained using the program Pymol.[69] Hydrogen bonds and van der Waals contacts were assigned with the program CONTACTSYM.[70,71] The cutoff for hydrogen bonds and salt bridges was 3.4 Å and up to 4.33 Å for van der Waals contacts, depending on atom type and using standard van der Waals contacts. The solvent accessibility of individual residues was assessed using the program MS[72,73] with a 1.4 Å radius for the solvent probe. Evaluation of the statistical per-atom score contributions were performed by using DrugScoreCSD[54,55]

Kinetic characterisation of the variants: K_i values were determined photometrically for each enzyme (wild-type bovine trypsin from Sigma, native recombinant bovine trypsin mutants prepared

as described above, and human factor Xa from Kordia Laboratory Supplies, Leiden, Netherlands) according to standard protocols[74] under the following conditions: 0.05 M Tris-HCl (pH 8.0), 0.154 M NaCl and 5% (*v*/*v*) ethanol, using different concentrations of the factor Xa substrate Pefachrome-tPA (Loxo GmbH, Dossenheim, Germany) at 25 °C. K_i values were determined as described by Dixon.[75]

Protein Data Bank accession numbers: Atomic coordinates have been deposited in the RCSB Protein Data Bank with the following entry codes: 99XbT·**1** complex, 1Y5U; 99XbT·**2** complex, 1Y59; 99XbT·**3** complex, 1Y5A; 99XbT·**4** complex, 1Y5B.

Acknowledgements

A.D.F. gratefully acknowledges the EU for a postdoctoral Marie Curie research training grant. The authors want to thank Prof. Dr. M. T. Stubbs (University of Halle, Germany) for helpful discussions and critical comments on the manuscript. We are grateful to Prof. Dr. Jörg Stürzebecher (University of Erfurt/Jena, Germany) for helpful discussions on the methodology to perform the kinetic measurements. We want to express our thanks to Dr. Daniel Rauh (Chemical Genomics Centre of the Max Planck Society, Germany) and Anastasia Tziridis (University of Halle, Germany) for the detailed introduction into the expression, refolding, and purification protocols of the mutants. The help of Dr. Marko Vogler (Microresist Technology, Berlin, Germany) for synthesizing the inhibitors studied in this contribution, is gratefully acknowledged. We thank the beamline support staff of the PSF at Bessy II for their help with data collection.

Keywords: aromatic interactions · crystal structures · factor Xa · inhibitors · selectivity · serine proteases

[1] V. A. Johnson, R. L. Smith, *Arch. Biochem. Biophys.* **1976**, *175*, 190 – 195.
[2] S. Maignan, V. Mikol, *Curr. Top. Med. Chem.* **2001**, *1*, 161 – 174.
[3] W. Bode, H. Brandstetter, T. Mather, M. T. Stubbs, *Thromb. Haemostasis* **1997**, *78*, 501 – 511.
[4] M. Renatus, W. Bode, R. Huber, J. Stürzebecher, M. T. Stubbs, *J. Med. Chem.* **1998**, *41*, 5445 – 5456.
[5] M. T. Stubbs, R. Huber, W. Bode, *FEBS Lett.* **1995**, *375*, 103 – 107.
[6] S. Maignan, J. P. Guilloteau, S. Pouzieux, Y. M. Choi-Sledeski, M. R. Becker, S. I. Klein, W. R. Ewing, H. W. Pauls, A. P. Spada, V. Mikol, *J. Med. Chem.* **2000**, *43*, 3226 – 3232.
[7] H. Brandstetter, A. Kühne, W. Bode, R. Huber, W. von der Saal, K. Wirthensohn, R. A. Engh, *J. Biol. Chem.* **1996**, *271*, 29 988 – 29 992.
[8] D. A. Dougherty, *Science* **1996**, *271*, 163 – 168.
[9] K. Schärer, M. Morgenthaler, R. Paulini, U. Obst-Sander, D. W. Banner, D. Schlatter, J. Benz, M. Stihle, F. Diederich, *Angew. Chem.* **2005**, *117*, 4474 – 4479; *Angew. Chem. Int. Ed.* **2005**, *44*, 4400 – 4404.
[10] J. P. Gallivan, D. A. Dougherty, *Proc. Natl. Acad. Sci. USA* **1999**, *96*, 9459 – 9464.
[11] M. Böhm, J. Stürzebecher, G. Klebe, *J. Med. Chem.* **1999**, *42*, 458 – 477.
[12] L. Serrano, M. Bycroft, A. R. Fersht, *J. Mol. Biol.* **1991**, *218*, 465 – 475.
[13] M. S. Cubberley, B. L. Iverson, *J. Am. Chem. Soc.* **2001**, *123*, 7560 – 7563.
[14] C. D. Tatko, M. L. Waters, *J. Am. Chem. Soc.* **2002**, *124*, 9372 – 9373.
[15] E. A. Meyer, R. K. Castellano, F. Diederich, *Angew. Chem.* **2003**, *115*, 1244 – 1287; *Angew. Chem. Int. Ed.* **2003**, *42*, 1210 – 1250; Corrigendum: E. A. Meyer, R. K. Castellano, F. Diederich, *Angew. Chem.* **2003**, *115*, 4254; *Angew. Chem. Int. Ed.* **2003**, *42*, 4120.
[16] E. T. Kool, *Annu. Rev. Biophys. Biomol. Struct.* **2001**, *30*, 1 – 22.
[17] N. Kannan, S. Vishveshwara, *Protein Eng.* **2000**, *13*, 753 – 761.
[18] E. Gazit, *FASEB J.* **2002**, *16*, 77 – 83.
[19] E. A. Padlan, *Proteins Struct. Funct. Genet.* **1990**, *7*, 112 – 124.
[20] A. Prochnicka-Chalufour, JL. Casanova, S. Avrameas, J. Claverie, P. Kourilsky, *Int. Immunol.* **1991**, *3*, 853–864.
[21] J. Singh, J. M. Thornton, *J. Mol. Biol.* **1990**, *211*, 1 – 6.
[22] T. Blundell, J. Singh, J. Thornton, S. K. Burley, G. A. Petsko, *Science* **1986**, *234*, 1005.
[23] J. B. O. Mitchell, C. L. Nandi, I. K. McDonald, J. M. Thornton, S. L. Price, *J. Mol. Biol.* **1994**, *239*, 315 – 331.
[24] A. G. Gillman, T. W. Rall, A. S. Mies, P. Taylor, *The Pharmaceutical basis of Therapeutics*, 8th ed., McGraw-Hill, New York, **1993**.
[25] S. Reyda, C. Sohn, G. Klebe, K. Rall, D. Ullmann, H. D. Jakubke, M. T. Stubbs, *J. Mol. Biol.* **2003**, *325*, 963 – 977.
[26] D. Rauh, S. Reyda, G. Klebe, M. T. Stubbs, *Biol. Chem.* **2002**, *383*, 1309 – 1314.
[27] D. Rauh, G. Klebe, J. Stürzebecher, M. T. Stubbs, *J. Mol. Biol.* **2003**, *330*, 761 – 770.
[28] D. Rauh, G. Klebe, M. T. Stubbs, *J. Mol. Biol.* **2004**, *335*, 1325 – 1341.
[29] J. T. den Dunnen, E. Antonarakis, *Hum. Genet.* **2001**, *109*, 121 – 124.
[30] M. Vogler, U. Koert, K. Harms, D. Dorsch, J. Gleitz, P. Raddatz, *Synthesis* **2004**, 1211 – 1228.
[31] B. A. Katz, J. M. Clark, J. S. Finer-Moore, T. E. Jenkins, C. R. Johnson, M. J. Ross, C. Luong, W. R. Moore, R. M. Stroud, *Nature* **1998**, *391*, 608 – 612.
[32] C. A. Hunter, J. K. M. Sanders, *J. Am. Chem. Soc.* **1990**, *112*, 5525 – 5534.
[33] C. A. Hunter, K. R. Lawson, C. J. Urch, *J. Chem. Soc. Perkin Trans. 2* **2001**, 651 – 669.
[34] P. Cársky, H. L. Selzle, E. W. Schlag, *Chem. Phys.* **1988**, *125*, 165 – 170.
[35] P. Hobza, H. L. Selzle, E. W. Schlag, *J. Chem. Phys.* **1990**, *93*, 5893 – 5897.
[36] W. L. Jorgensen, D. L. Severance, *J. Am. Chem. Soc.* **1990**, *112*, 4768 – 4774.
[37] P. Linse, *J. Am. Chem. Soc.* **1992**, *114*, 4366 – 4373.
[38] P. Hobza, H. L. Selzle, E. W. Schlag, *J. Phys. Chem.* **1993**, *97*, 3937 – 3938.
[39] R. L. Jaffe, G. D. Smith, *J. Chem. Phys.* **1996**, *105*, 2780 – 2788.
[40] G. D. Smith, R. L. Jaffe, *J. Phys. Chem.* **1996**, *100*, 9624 – 9630.
[41] C. Chipot, R. Jaffe, B. Maigret, D. A. Pearlman, P. A. Kollman, *J. Am. Chem. Soc.* **1996**, *118*, 11 217 – 11 224.
[42] P. Hobza, H. L. Selzle, E. W. Schlag, *J. Phys. Chem.* **1996**, *100*, 18 790 – 18 794.
[43] K. C. Janda, J. C. Hemminger, J. S. Winn, S. E. Novik, S. J. Harris, W. Klemperer, *J. Chem. Phys.* **1975**, *63*, 1419 – 1421.
[44] J. M. Steed, T. A. Dixon, W. Klemperer, *J. Chem. Phys.* **1979**, *70*, 4940 – 4946.
[45] R. Laatikainen, J. Ratilainen, R. Sebastian, H. Santa, *J. Am. Chem. Soc.* **1995**, *117*, 11 006 – 11 010.
[46] D. Hall, D. E. Williams, *Acta Crystallogr. Sect. A* **1975**, *31*, 56 – 58.
[47] P. R. R. Langridge-Smith, D. V. Brumbaugh, C. A. Haynam, D. H. Levy, *J. Phys. Chem.* **1981**, *85*, 3742 – 3746.
[48] D. H. Levy, C. A. Haynam, D. V. Brumbaugh, *Faraday Discuss. Chem. Soc.* **1982**, *73*, 137 – 151.
[49] S. L. Price, A. J. Stone, *J. Chem. Phys.* **1987**, *86*, 2859 – 2868.
[50] S. K. Burley, G. A. Petsko, *Science* **1985**, *229*, 23 – 28.
[51] G. B. McGaughey, M. Gagné, A. K. Rappé, *J. Biol. Chem.* **1998**, *273*, 15 458 – 15 463.
[52] G. Alagona, C. Ghio, S. Monti, *J. Phys. Chem. A* **1998**, *102*, 6152 – 6160.
[53] R. Chelli, F. L. Gervasio, P. Procacci, V. Schettino, *J. Am. Chem. Soc.* **2002**, *124*, 6133 – 6143.
[54] H. Gohlke, M. Hendlich, G. Klebe, *J. Mol. Biol.* **2000**, *295*, 337 – 356.
[55] H. Velec, H. Gohlke, G. Klebe, *J. Med. Chem.* **2005**, *48*, 6296 – 6303.
[56] G. Kryger, I. Silman, J. L. Sussman, *J. Physiol.* **1998**, 92, 191 – 194.
[57] G. Kryger, I. Silman, J. L. Sussman, *Structure* **1999**, *7*, 297 – 307.
[58] P. Betschmann, S. Sahli, F. Diederich, U. Obst, V. Gramlich, *Helv. Chim. Acta* **2002**, *85*, 1210 – 1245.
[59] U. Obst, D. W. Banner, L. Weber, F. Diederich, *Chem. Biol.* **1997**, *4*, 287 – 295.
[60] Z. H. Song, C. A. Slowey, D. P. Hurst, P. H. Reggio, *Mol. Pharm.* **1999**, *56*, 834 – 840.
[61] C. Papworth, J. C. Bauer, J. Braman, D. A. Wright, **1996**, *9*, 3 – 4.
[62] R. Rudolph, G. Böhm, H. Lilie, R. Jaenicke in *Protein Structure, A Practical Approach*, 2nd ed. (Eds.: T. E. Creighton), Oxford University Press, Oxford, **1996**, pp. 57 – 99.
[63] Z. Otwinowski, W. Minor in *Methods in Enzymology, Vol. 276A* (Eds.: C. W. Carter, Jr., R. M. Sweet), New York, Academic Press, **1997**, pp. 307 – 326.

[64] J. Navaza, *Acta Crystallogr. Sect. A* **1994**, *50*, 157 – 163.
[65] Collaborative Computational Project, Number 4, *Acta Crystallogr. Sect. D* **1994**, *50*, 760 – 763.
[66] A. T. Brunger, P. D. Adams, G. M. Clore, P. Gros, R. W. Grosse-Kunstleve, J.-S. Jiang, J. Kuszewski, N. Nilges, N. S. Pannu, R. J. Read, L. M. Rice, T. Simonson, G. L. Warren, *Acta Crystallogr. Sect. D* **1998**, *54*, 905 – 921.
[67] G. M. Sheldrick, T. R. Schneider in *Methods in Enzymology, Vol. 277* (Eds.: R. M. Sweet, C. W. Carter, Jr.), Academic Press, Orlando, FL, **1997**, pp. 319 – 343.
[68] T. A. Jones, J. Y. Zou, S. W. Cowan, M. Kjeelgaard, *Acta Crystallogr. Sect. A* **1991**, *47*, 110 – 119.
[69] W. L. DeLano, DeLano Scientific, San Carlos, CA, USA, **2002**, http://www.pymol.org.
[70] S. Sheriff, W. A. Hendrickson, J. L. Smith, *J. Mol. Biol.* **1987**, *197*, 273 – 296.
[71] S. Sheriff, *Immunomethods* **1993**, *3*, 191 – 196.
[72] M. L. Connolly, *J. Appl. Crystallogr.* **1983**, *16*, 548 – 558.
[73] M. L. Connolly, *Science* **1983**, *221*, 709 – 713.
[74] J. Stürzebecher, U. Stürzebecher, H. Vieweg, G. Wagner, J. Hauptmann, F. Markwardt, *Thromb. Res.* **1989**, *54*, 245 – 252.
[75] M. Dixon, *Biochem. J.* **1972**, *129*, 197 – 202.
[76] R. A. Laskowski, M. W. MacArthur, D. S. Moss, J. M. Thornton, *J. Appl. Crystallogr.* **1993**, *26*, 283 – 291.

Received: July 28, 2006
Published online on December 27, 2006

